RAPID COMMUNICATIONS

PHYSICAL REVIEW B VOLUME 47, NUMBER 15 15 APRIL 1993-I

Critical test of the structure of the ordered phase in epitaxially grown Si_xGe_{1-x} films

F. K. LeGoues, R. M. Tromp, V. P. Kesan, and J. Tsang
IBM Research Division, Thomas J. Watson Research Center, Yorktown Heights, New York 10598
(Received 18 September 1992; revised manuscript received 28 December 1992)

Two different structural models have been recently proposed to explain the ordering observed in Si_xGe_{1-x} alloys grown at low temperatures on Si(001). We show that, through dark field imaging of the different domains of the ordered phase, it is possible to differentiate between the two structures unequivocally. In this way, we determine that the ordered phase corresponds to ordering along a single set of {111} planes, where Ge-rich double layers alternate with Si-rich double layers. We also show that this conclusion is consistent with all other experimental data reported so far.

Ordering in Si_xGe_{1-x} thin films grown on Si(001) substrates has been reported by several groups in recent years,[1-3] and has led to a great deal of interest, primarily because Si_xGe_{1-x} alloys were, up to that point, thought to behave as an almost ideal solid solution. It was then shown[4] that the observed order is not an equilibrium feature of the alloy, but a result of the specific configuration of the growth surface. Based on this observation, LeGoues *et al.* (LKITT) proposed a model based on equilibrium, strain-induced lateral surface segregation, frozen in during growth.[4] Unlike previously proposed structural models, the LKITT structure is internally strained and consists of alternating double {111} layers of Si and Ge [Fig. 1(a)]. This model was shown to be consistent with the observed intensities of the electron diffraction patterns obtained from the alloys. More recently, an alternate explanation for the observations was proposed by Jesson *et al.*,[5] where ordering in Si_xGe_{1-x} alloys was explained by segregation at step edges during growth of the alloys. This again accounts for both the nonequilibrium nature of the ordered alloy, and the nonreversibility of the ordering. The structural model proposed by Jesson *et al.*[5] (JPBH) differs from the LKITT model because it is ordered simultaneously along two different {111} planes [Fig. 1(b)]. The JPBH model assumes that growth occurs by the motion of single steps, while the LKITT model assumes the motion of double steps. Since it is not known experimentally which one of these is more likely [an argument for either possibility can be made based on data obtained for the growth of Si on Si(001) (Ref. 6)], the only way of distinguishing between the two models is to experimentally determine which of the structures is consistent with observed data.

In this paper we show conclusively, through dark field imaging of the different domains in several zones axes, that the LKITT model is the only model consistent with experimental data. We further review extensive data obtained by Kesan, LeGoues, and Iyer[7] and by Tsang *et al.*,[8] where the amount of ordering was quantified by x-ray diffraction and Raman scattering, respectively. Although the x-ray data are consistent with both the LKITT and JPBH models, the Raman data can only be explained by the LKITT model. Finally, we show that the data presented by JPBH as proof of their mechanism's validity are fully consistent with the LKITT mechanism.

The sample used for this study was similar to that used in Refs. 3, 4, 7, and 8, and consisted of 0.5 μm of $Si_{0.5}Ge_{0.5}$ grown by molecular-beam epitaxy at 450 °C. These are similar conditions to those used in the JPBH study. The TEM samples were prepared for planar view observation by mechanical thinning, followed by ion milling at liquid-nitrogen temperature. The observations were performed in a Philips 420 TEM operating at 120 kV.

The structural models proposed by LKITT and by JPBH are shown schematically in Fig. 1. In the LKITT model, Ge-rich double {111} layers alternate with Si-rich double {111} layers. In this case, the order parameter is defined as the difference in composition between the Ge-rich and Si-rich double layers. The JPBH model is more complicated since order occurs in two different {111} planes, chosen so that their intersections with the (001) plane are orthogonal to each other [for example, order along the (111) and the $(1\bar{1}1)$ planes]. The sequence of {111} planes along one of the ordered directions is thus Ge-rich, average composition, Si-rich, average composition, ... Of course, the plane of average composition is actually ordered along the other {111} plane, as shown in Fig. 1(b). The JPBH order parameter can be obtained similarly to the LKITT model, as the difference in composition between the single Ge-rich and Si-rich planes, but this order parameter applies to the two ordering directions. Both models are expected to form four

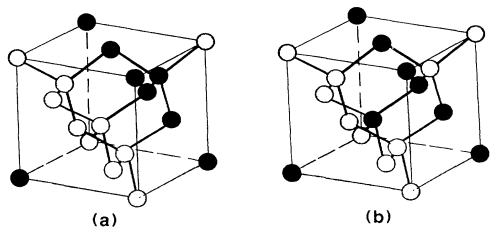

FIG. 1. Schematic models of the two structures discussed in this paper. (a) LKITT model, (b) JPBH model. Note that, for both structures, only one-eighth of the unit cell has been represented.

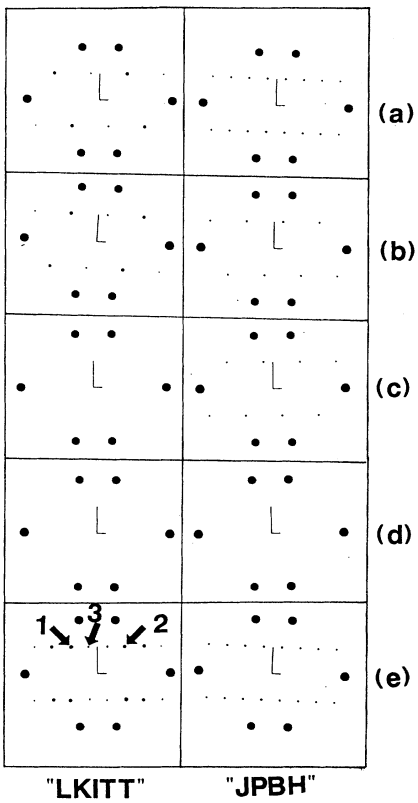

FIG. 2. Simulated electron diffraction patterns, for the [013] zone axis, for both structures, for all possible domains. (a)–(d) Diffraction patterns for the four individual domains. (e) Superimposition of the diffraction patterns for the four domains. [Note that the reflections due to double diffraction in the Si_xGe_{1-x} lattice are not included in the simulation, i.e., the (200)-type spots are not present.]

domains: for the LKITT model, these correspond to ordering along the four {111} planes. For the JPBH model, the four domains correspond to the four ways of combining the {111} planes in suitable pairs. As expected, the electron diffraction patterns obtained from these two structure are similar, but nonetheless display important differences. Figure 2 shows the diffraction patterns calculated for the four domains, for both structures, in the [013] zone axis. The expected experimental diffraction pattern corresponds to the superimposition of the patterns for the four domains, and is included in Fig. 2. The differences between the experimental patterns expected for the LKITT and JPBH structures are thus rather subtle. But we note that for the JPBH model, reflections marked 1 (or 2) and 3 have equal intensities, while the LKITT structure predicts observable differences in intensities between 1 (or 2) and 3. In Ref. 1, the nonequilibrium nature of the structure was actually determined by pointing out these differences in the experimental patterns. This can also be observed on the diffraction pattern included in Fig. 3(e), where spot 3 is noticeably weaker than spots 1 or 2.

Furthermore, since, unlike the superimposed patterns, the individual diffraction patterns show significant differences between the two structures, it is possible to differentiate between them by dark field microscopy. For the LKITT model, dark field imaging using spots 1 and 2 (on Figs. 2 and 3) in the [013] zone axis would highlight domains two and one, respectively. Similarly, the equivalent spots on the $[0\bar{1}3]$ zone axis would highlight domains three and four. In other words, by obtaining four dark field images, on spots 1 and 2 of both the [013] and the $[0\bar{1}3]$ zone axes, only *one,* unique domain would be imaged in each case. On the other hand, for the JPBH model, dark field imaging in the [013] zone axis on spot 1

TABLE I. Measured area fractions highlighted in each of the dark fields of Fig. 3, total area ordered, and measured overlap between the highlighted areas (all measurements were obtained from the digitized images and their superimposition, except for the total amount ordered, which was obtained from x-ray and Raman measurements). The theoretical predictions are obtained by assuming that each dark field highlights either one or two domains at a time, depending on the model.

Area fractions highlighted in Figs. 3(a)–3(d)	Percentage of sample ordered in each domain assuming LKITT	Percentage of sample ordered in each domain assuming JPBH
18	18	14
22	22	9
24	24	15
23	23	9

Values predicted assuming each model	LKITT	JPBH	Measured
Total area ordered	88%	47%	80.00% (determined by x-ray and Raman measurements)
Overlap between dark fields 3(a) and 3(d)	0%	14%	2%
Overlap between dark fields 3(b) and 3(d)	0%	9%	2%
Overlap between dark fields 3(a) and 3(c)	0%	14%	1%
Overlap between dark fields 3(c) and 3(d)	0%	15%	2%

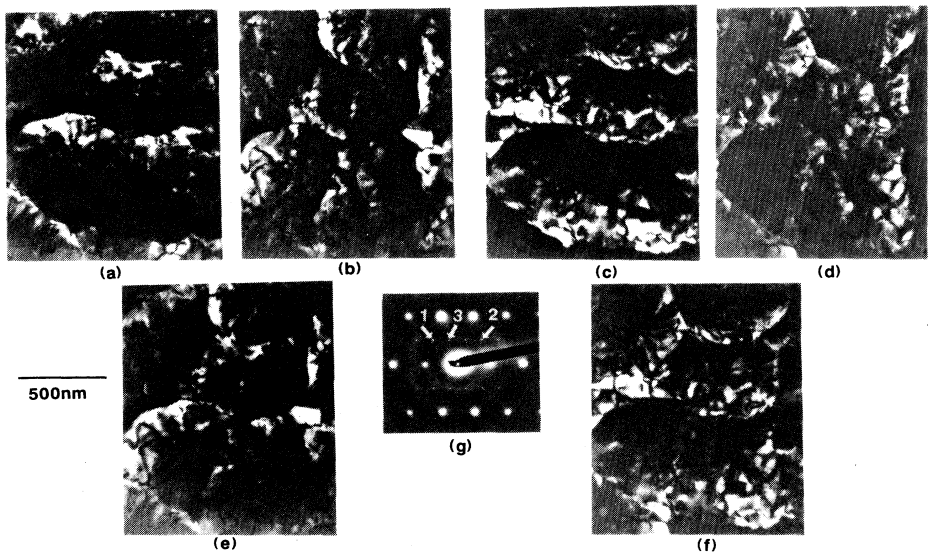

FIG. 3. Experimental dark field images obtained from spots marked 1 and 2 (on the diffraction pattern included in the bright field image) in the [013] and the [0$\bar{1}$3] zone axes. (a) and (b) Dark field images obtained in the [013] zone axis, using spots 1 and 2, respectively. (c) and (d) Dark field images, obtained in the [0$\bar{1}$3] zone axis, using spots 1 and 2, respectively. (e) Superimposition of (a) and (b). (f) Superimposition of (c) and (d). [(e) and (f) were obtained by laying the two negatives on top of each other and printing a picture of both at the same time.] (g) Experimental [013] diffraction pattern showing the superlattice reflections used for the dark field. Note the spot marked 3 is significantly weaker than either 1 or 2.

would highlight domains 1 and 2 simultaneously, while dark field imaging on spot 2 would highlight domains 1 and 3 simultaneously. Similarly, in the [0$\bar{1}$3] zone axis, spot 1 would highlight domains 4 and 2 and spot 2 would highlight domains 4 and 3. Thus for the JPBH structure dark field imaging on spots 1 and 2, for both zone axes, would always highlight *two* domains at a time. It is then easy to distinguish between the two structures, by checking whether the dark field images behave one way or the other. Figure 3 shows dark field images obtained for spots 1 and 2, both in the [013] and the [0$\bar{1}$3] zone axes. Figures 3(a)–3(d) show the four individual dark fields micrographs, obtained using spots 1 and 2 in both the [013] and the [0$\bar{1}$3] zone axes. Figure 3(e) shows the superimposition of Figs. 3(a) and 3(b), while Fig. 3(f) shows the superimposition of Figs. 3(c) and 3(d). It is readily apparent that the four micrographs have highlighted four different domains, and not two at a time. Further, Figs. 3(e) and 3(f) have very little common areas highlighted, and almost look like negative versions of each other, showing again that each dark field image highlights only one domain at a time.

We have digitized and binarized the micrographs in order to quantify the area fraction highlighted in each dark field, so as to more directly compare the data with the results expected for each model. We thus determine that the area fractions highlighted by the four dark fields in Fig. 3 are, respectively, 18%, 22%, 23%, and 24%. Assuming each model in turn, we calculated the percentage ordered in each of the four domains. We also measured the overlap between the different domains, and compared these values with those expected for the two models. This is presented in Table I. We first note that, since the JPBH model would result in highlighting two domains at a time, the total percentage of ordered phase in this assumption is only 47%. This is inconsistent with x-ray and Raman results (see next paragraph and Refs. 7 and 8). Further, the LKITT model predicts no overlap between the different dark fields, while the JPBH model would result in considerable overlap. Table I shows that we measure very little overlap between the different highlighted areas. This analysis was performed for two areas each in two different samples, showing very similar results. This shows that the LKITT structure, but not the JPBH structure, is consistent with the experimental data.

We now review other, published data, which further confirm this conclusion. It was pointed out by LKITT and JPBH that "perfect" order (order parameter equals 1) was unlikely due to the highly nonequilibrium nature of the ordering phenomenon. The order parameter was determined from grazing angle x-ray diffraction measurements of the ratio (R) of intensities between the forbidden 1/2(7,7,7) peak and the 1/2(8,8,8) peak[7] (corrected for the geometry of the experiment). $\sqrt{R}$ is equal to the ratio of the 1/2(7,7,7) and 1/2(8,8,8) structure factors (as appropriate for each model), multiplied by the order parameter. Thus, for each model, the order parameter can be determined directly from R. The measured order parameter for the LKITT model equals 0.65 (assuming the sample is ordered over its entire area), corresponding to double layers containing 82% Ge alternating with double layers containing 18% Ge. For the JPBH model, one has to be careful to account for the ordering along the two

{111} planes, by dividing the measured intensity in two. R is then found to be equal to 0.6 which again corresponds to single layers containing 80% Ge alternating with single layers containing 20% Ge, but in two directions. Thus, the x-ray diffraction measurement can be explained by either structure.

On the other hand, Raman scattering was also used to independently determine the order parameter. In Ref. 8, the Raman spectra of compositionally order $Si_{0.5}Ge_{0.5}$ alloys were measured, and compared to the corresponding random alloy. The changes in relative intensities of the different optical phonons were used to quantify the amount of ordering. It was thus found that the order parameter for the LKITT model is equal to 0.64, in very good agreement with the order parameter obtained from x-ray measurements. Since the Raman-scattering experiment effectively "counts" Si-Si, Ge-Ge, and Si-Ge bonds, it is not sensitive, as x-ray diffraction was, to the orientation of all possible domains. If we assume the JPBH structure, the Raman measurements result in an ordering parameter of 1.0, which is inconsistent with the x-ray data, as well as extremely unlikely considering the highly kinetic nature of the phenomenon. The Raman data are thus only consistent with the LKITT model.

We now show that the JPBH data are consistent with the LKITT model. Indeed, the simulation shown on Fig. 1(b) in Ref. 5 as evidence for the JPBH model was performed using the "perfect" ordered structure shown in Fig. 1(b). Since pairs of atoms are imaged, not individual ones, this is equivalent to simulating double layers containing, on average 75% Ge (average between one pure Ge plane and one plane containing 50% Ge) alternating with double layers containing, on average, 25% Ge. These values are very close to those determined experimentally[7,8] (see above). By contrast, as shown in Fig. 3 in Ref. 5, the JPBH order parameter is expected to be much lower, with a maximum of about 0.30, which corresponds to double planes containing 57.5% Ge alternating with double planes containing 42.5% Ge. Thus, the Z-contrast analysis is not inconsistent with the LKITT model. Further, it was pointed out in Ref. 7 that the amount of ordering is extremely dependent on the exact growth conditions, and on the average amount of Ge in the alloy. Optimum ordering was only obtained for alloys containing 50% Ge, and the order parameter decreased sharply on either side of this composition.[7] The alloys in the JPBH study contained only 40% Ge, so that maximum ordering should not have been expected. Thus, an image showing less order than expected does not disprove the LKITT model, but can straightforwardly be explained by poor ordering in the particular sample.

We have shown by dark field electron microscopy that the LKITT model for the ordered Si_xGe_{1-x} alloy agrees well with the experiment, while the JPBH model is *qualitatively* inconsistent with these results. The LKITT model can also satisfactorily account for both the x-ray diffraction and Raman-scattering experiments. Finally, Z-contrast images presented as proof of the JPBH model are easily explained by the LKITT model.

[1]A. Ourmazd and J. C. Bean, Phys. Rev. Lett. **55**, 765 (1985).
[2]D. J. Lockwood, K. Rajan, E. W. Fenton, J.-M. Baribeau, and M. W. Denhoff, Solid State Commun. **61**, 465 (1987).
[3]F. K. LeGoues, V. P. Kesan, and S. S. Iyer, Phys. Rev. Lett. **64**, 40 (1990).
[4]F. K. LeGoues, V. P. Kesan, S. S. Iyer, J. Tersoff, and R. M. Tromp, Phys. Rev. Lett. **64**, 2038 (1990).
[5]D. E. Jesson, S. J. Pennycook, J.-M. Baribeau, and D. C. Houghton, Phys. Rev. Lett. **68**, 2062 (1992).
[6]A. J. Hoeven *et al.*, Thin Solid Films **183**, 263 (1989); R. J. Hamers, U. K. Kohller, and J. E. Demuth, J. Vac. Sci. Technol. A **8**, 195 (1990).
[7]V. P. Kesan, F. K. LeGoues, and S. S. Iyer, Phys. Rev. B **46**, 1576 (1992).
[8]J. C. Tsang, V. P. Kesan, J. L. Freeouf, F. K. LeGoues, and S. S. Iyer, Phys. Rev. B **46**, 6907 (1992).

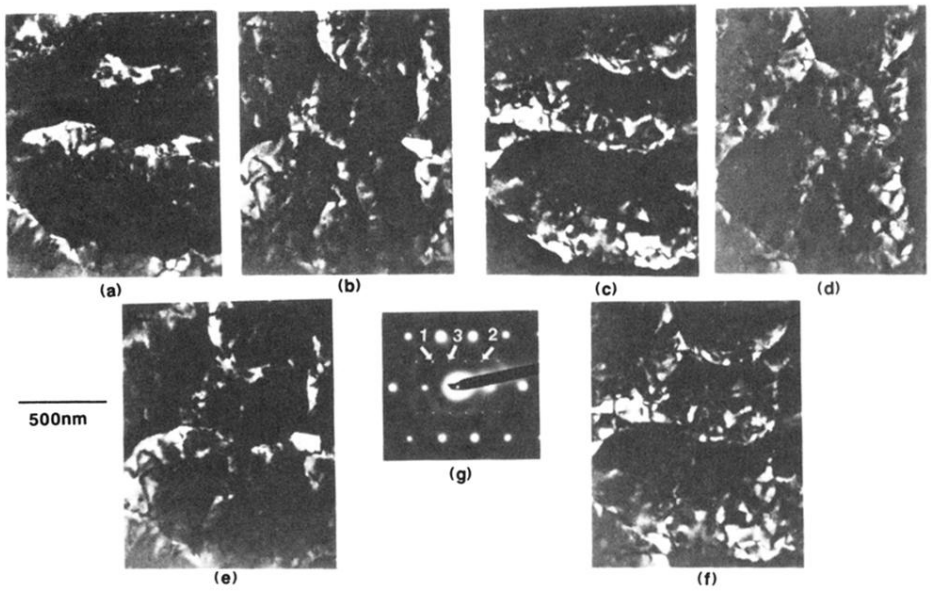

FIG. 3. Experimental dark field images obtained from spots marked 1 and 2 (on the diffraction pattern included in the bright field image) in the [013] and the $[0\bar{1}3]$ zone axes. (a) and (b) Dark field images obtained in the [013] zone axis, using spots 1 and 2, respectively. (c) and (d) Dark field images, obtained in the $[0\bar{1}3]$ zone axis, using spots 1 and 2, respectively. (e) Superimposition of (a) and (b). (f) Superimposition of (c) and (d). [(e) and (f) were obtained by laying the two negatives on top of each other and printing a picture of both at the same time.] (g) Experimental [013] diffraction pattern showing the superlattice reflections used for the dark field. Note the spot marked 3 is significantly weaker than either 1 or 2.